Numerical study on an application of subwavelength dielectric gratings for high-sensitivity plasmonic detection

Woo Kyung Jung, Nak-Hyeon Kim, and Kyung Min Byun*

Department of Biomedical Engineering, Kyung Hee University, Yongin, 446-701, South Korea

*Corresponding author: kmbyun@khu.ac.kr

Received 22 March 2012; revised 16 May 2012; accepted 21 May 2012;
posted 22 May 2012 (Doc. ID 165300); published 9 July 2012

Although subwavelength dielectric gratings can be employed to achieve a high sensitivity of the surface plasmon resonance (SPR) biosensor, the plasmonic interpretation verifying the resulting sensitivity improvement remains unclear. The aim of this study is to elucidate the effects of the grating's geometric parameters on the amplification of SPR responses and to understand the physical mechanisms associated with the enhancement. Our numerical results show that the proposed SPR substrate with a dielectric grating can provide a better sensitivity due to the combined effects of surface reaction area and field distribution at the binding region. An influence of adhesion layer on the sensor performance is also discussed. The obtained results will be promising in high-sensitivity plasmonic biosensing applications.

OCIS codes: 050.6624, 240.6680, 280.4788.

1. Introduction

The surface plasmon resonance (SPR) biosensor has gained much attention because it allows label-free and quantitative detection of biomolecular interactions in real-time [1]. The SPR technique is based on a coupling between incident light and free electrons in metal. When a momentum of incident light matches that of free electrons, the light energy is completely absorbed and converted into a collective oscillation of the free electrons, called surface plasmons (SPs). Since this coupling condition is dependent on the refractive index of a dielectric medium surrounding the metal surface, one can monitor the binding events of biomolecules by measuring the shift of resonance angle or wavelength. The SPR sensor system typically uses the Kretschmann configuration, where a thin metallic film prepared on a glass substrate is attached to a prism coupler via index-matching oil.

Among several issues related to the SPR biosensor, improvement of sensor sensitivity has been one of the recent trends of theoretical and experimental studies. Together with the efforts toward multiplexing and miniaturization, a variety of researches have been conducted to answer the question of how the plasmon excitation can be used advantageously in order to overcome the sensitivity limit of traditional SPR sensing devices [2]. In our previous investigations, use of periodic metallic nanostructures built on a thin metal film resulted in a significant SPR signal amplification [3,4]. This approach could serves as an effective way to increase a surface reaction area and to generate a locally enhanced field by a resonant excitation of localized surface plasmon (LSP) modes. Since any corrugation, even at the nanometer scale, can provide more binding spaces than an ideally flat surface, introduction of metallic nanostructures can increase the number of ligands and target molecules that participate in the binding interactions, therefore, producing a higher resonance shift. Furthermore, when adsorbed biomolecules are exposed to localized plasmon fields, the resonance shift

1559-128X/12/204722-08$15.00/0

as a result of the biointeraction could be stronger. This interesting correlation between local field enhancement and SPR signal amplification has been verified both theoretically and experimentally [5,6]. Moreover, the periodic metallic nanostructures can be customized as desired to meet the specific sensitivity requirements.

Despite these advantageous aspects, it has been found that metallic nanostructures make the SPR curve broader and shallower inevitably [7]. This deformation of SPR characteristics can increase the uncertainty of the sensor output and affect its high standard error in experimental measurement. Moreover, as a notable amplification in local field intensity is generally found at the sharp edges of the metallic nanostructures, guided ligand immobilization and target localization into such regions with a highly enhanced field are essential for preventing the biomolecules from being wasted in the weak field [8].

Recently, there has been special attention being paid to an alternative approach based on nonabsorbing dielectric structures. For example, dielectric structures with a high pore volume could simply improve the sensor sensitivity by increasing the surface reaction area [9]. Although nonabsorbing materials on a thin metal film may induce a slightly broader curve width because of resonant excitations at a higher plasmon angle, the dielectric overlayers possessing a negligible extinction coefficient do not prompt an absorptive plasmon damping. Hence, optimization of dielectric nanostructures can be an effective approach for providing an enhanced sensitivity while preventing the signal quality from being degenerated significantly.

In this study, we intend to demonstrate the SPR signal enhancement induced by a periodic dielectric nanostructure. For this purpose, subwavelength dielectric gratings are employed and their plasmonic effects on the sensor sensitivity are explored. More specifically, to assess the sensing performance of the plasmonic substrate with dielectric gratings, the SPR characteristics are investigated quantitatively for a wide range of grating periods and thicknesses. The results of this study could show a possibility of improving and optimizing the nanostructured plasmonic substrates for sensitive SPR detection of biointeractions.

2. Numerical Model

Figure 1 shows a schematic diagram of the proposed SPR biosensor. A thin gold film with a thickness of 45 nm is coated on an SF10 glass prism via an attachment of 2 nm thick chromium layer. One-dimensional rectangular grating with a period of Λ and a thickness of d_g is regularly patterned on the gold/SF10 glass substrate supporting the SP waves. A biomolecular reaction occurring at the grating surface is modeled as a 2 nm thick dielectric layer that covers the whole sensor surface. The refractive index of the binding layer (n_{BL}) is set to be 1.40 for ligand immobilization, and this value increases up to 1.50 with the interaction between capture and target probes. This refractive index change is based on the measurement data obtained from ellipsometric characterizations for DNA hybridization [10]. TM-polarized light at the wavelength $\lambda = 633$ nm illuminates the substrate. The optical constants $\varepsilon = (n, k)$ of SF10 substrate, thin layers of chromium and gold, and dielectric gratings are set to be (1.723, 0), (3.48, 4.36), (0.18, 3.00), and (1.50, 0) [e.g., polymethyl methacrylate (PMMA)], respectively, at $\lambda = 633$ nm [11]. Also, the refractive index of a phosphate buffered saline (PBS) solution is assumed to be 1.33.

For numerical simulations, we employ the rigorous coupled-wave analysis (RCWA) method, which has successfully been used to explain the experimental results of grating structures [12]. Our RCWA routine was proved to corroborate the experiments of earlier SPR studies based on various periodic nanostructures. Note that, since the field varies more rapidly in short distances of a grating with a size smaller than a wavelength λ, more space-harmonic orders are required to achieve the convergence and to improve the accuracy in calculations [13]. For the calculation presented in this study, 30 spatial harmonics

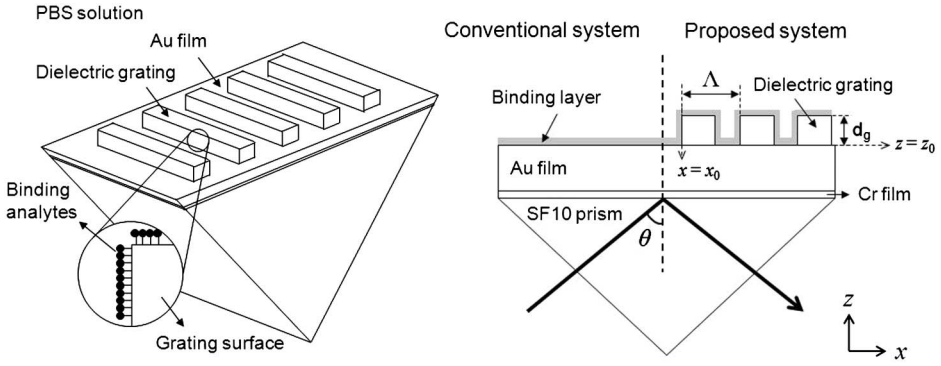

Fig. 1. Perspective view of the proposed SPR sensing configuration and its cross-sectional image. TM-polarized light with $\lambda = 633$ nm is incident through a gold/chromium/SF10 substrate with an angle of θ. Dielectric gratings are regularly patterned on the 45 nm thick planar gold film in PBS solution. The grating structure of a rectangular profile has a period of Λ and a thickness of d_g. A 2 nm thick binding layer is assumed to cover the whole sensor surface uniformly.

have been considered and convergence in RCWA computation was successfully achieved.

As a quantitative measure of the sensitivity improvement, we make use of the sensitivity enhancement factor (SEF), which is the ratio of the SPR angle shift due to the refractive index change in the 2 nm thick binding layer on the proposed SPR substrate with dielectric gratings to that of a conventional one. While SPR curves for a conventional SPR system are not shown, the resonance angles are obtained to be 59.75° for $n_{\mathrm{BL}} = 1.40$ and 59.94° for $n_{\mathrm{BL}} = 1.50$ in PBS solution; thus, the reference resonance shift is 0.19°.

3. Numerical Results

A. Effect of Grating Thickness on Sensitivity Enhancement

Figure 2 shows the SPR characteristics of the proposed SPR structure when a dielectric grating has a period of $\Lambda = 100$ nm and a width of 50 nm (i.e., a fill factor $f = 0.5$). As a grating thickness d_g increases from 0 to 200 nm with a step of 10 nm, resonance angle tends to increase gradually because the growing d_g causes a local refractive index surrounding the metal film to be effectively increased. Also, a strong dependence of the sensitivity on d_g is obvious. At an initial stage, the SPR angle shift presents a growing trend because the surface reaction area is increased with the grating thickness. However, when d_g exceeds 100 nm, a slope of the SPR angle shift becomes decreased and then saturates at $d_g > 150$ nm. No further growth in sensitivity can be explained by the limited penetration depth of propagating plasmon waves with exponentially decaying intensity. Since the detection range of an SPR biosensor is confined to the penetration depth [14], an increase of d_g over the plasmon decay length can no longer make contributions to the sensitivity enhancement.

What will follow is the correlation study between the surface reaction area and the sensitivity improvement. To quantify the effect of the surface-limited increase of a binding area on the enhanced sensitivity, the surface area growth factor (SAGF), the ratio of the surface reaction area of dielectric grating-based SPR substrates to that of a conventional SPR substrate, is employed. Although the binding layer is assumed to cover an infinite sensor surface, the SAGF can be derived regardless of the surface dimension because the reaction area per period can be substituted for the binding events over the whole sensor surface. Based on the geometric parameters shown in Fig. 1, we can obtain the expression of SAGF $= (\Lambda + 2d_g)/\Lambda$.

Direct comparison between SEF and SAGF in Fig. 3 exhibits that the SEF increases with a grating thickness until it reaches a maximum of 3.00. SEF is well in accord with the SAGF when a grating is relatively thin; however, a discrepancy between them grows significantly at $d_g > 80$ nm. It is associated with the fact that the influence of binding events on the sensitivity characteristic becomes worse for thick gratings due to an exponentially decaying evanescent field. In this regard, we should recognize the need for considering an impact of plasmon field distribution on the sensor sensitivity. It is, thus, believed that the sensor sensitivity is not governed only by an increased surface area, but rather by both the reaction area and the field distribution. The first-order perturbation theory by Abdulhalim also supports this interpretation, in that maximizing the sensor sensitivity can be accomplished by increasing the interaction volume or by increasing the field intensity in the analyte region [15]. As a result, an overlap integral (OI) can be more useful in analyzing the sensitivity characteristic than SAGF, which is given by

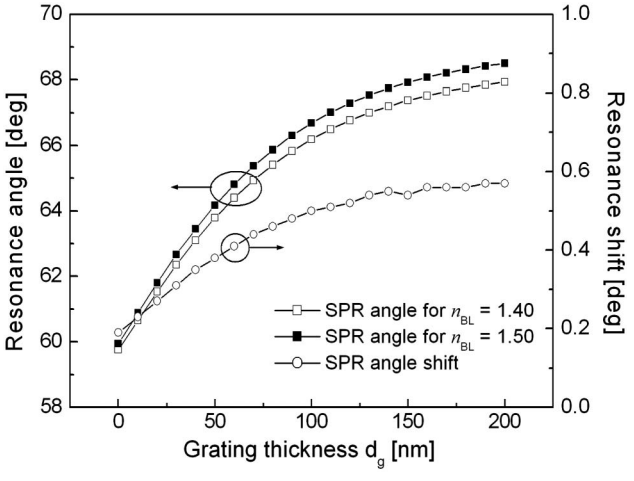

Fig. 2. Resonance angles (rectangles) and sensitivity characteristic (circle) for an SPR structure with dielectric gratings of $\Lambda = 100$ nm and a fill factor $f = 0.5$ when the refractive index of the binding layer increases from 1.40 to 1.50. The grating thickness d_g varies from 0 to 200 nm with a step of 10 nm.

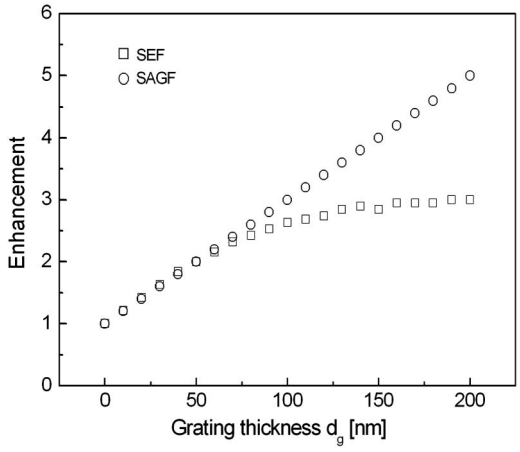

Fig. 3. Comparison between SEF (rectangles) and SAGF (circles) when the grating thickness increases from 0 to 200 nm. The geometric parameters of a dielectric grating are the same as those in Fig. 2.

$$\mathrm{OI} = \frac{1}{\Lambda} \int_{x=x_0}^{x=x_0+\Lambda} \int_{z=z_0}^{z=z_0+\lambda} \Delta n_{\mathrm{BL}} \cdot |E_X(x,z)|^2 \mathrm{d}z\mathrm{d}x, \quad (1)$$

where x and z represent the horizontal and vertical axes in Fig. 1. The integral boundary in z-axis ranging from z_0 to $z_0 + \lambda$ is determined from the fact that the plasmon field is evanescent and the amplitude decays approximately to zero after moving the distance of one wavelength from a gold surface. Δn_{BL} is the refractive index change caused by the binding event of target molecules. In our numerical model, $\Delta n_{\mathrm{BL}} = 0.1$ within the interaction area and otherwise, $\Delta n_{\mathrm{BL}} = 0$. Briefly, the OI directly addresses the combined effects of surface reaction area and field distribution on the sensitivity enhancement.

We have computed the near-field intensity using the finite-difference time-domain (FDTD) method. The FDTD results in Fig. 4 show that the field amplitude reaches a maximum at the metal surface and then falls exponentially along the z-axis. The peak amplitude of E_X is, respectively, obtained to be 3.8 for $d_g = 0$ nm, 5.1 for $d_g = 100$ nm, and 5.5 for $d_g = 200$ nm. This slight increment of the peak value may partially contribute to the sensitivity improvement with a growing d_g, although the field enhancement appears less significant compared with the LSP modes produced by metallic nanostructures.

Enhancement comparison of SEF, SAGF, and OI enhancement factor (OIEF) is demonstrated in Table 1. For unit period of $\Lambda = 100$ nm, a traditional SPR system without dielectric gratings is determined to have $\mathrm{OI}_{\mathrm{Control}} = 14.43$ by Eq. (1) and thus, OIEF can be defined as the ratio of the OI obtained from the SPR structure with dielectric gratings to the $\mathrm{OI}_{\mathrm{Control}}$. Since the OIs of $d_g = 100$ and 200 nm are equal to 34.33 and 41.82, the OIEF is 2.4 for $d_g = 100$ nm and 2.9 for $d_g = 200$ nm, respectively. When the three enhancement factors are directly compared, it is evidently found that the SEF is more consistent with the OI than the SAGF. Strong correlation between SEF and OI shows an interesting possibility that an evaluation of a near-field quantity can predict the far-field performance, such as sensor sensitivity.

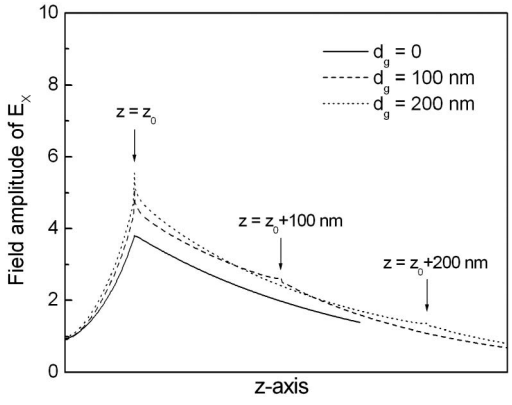

Fig. 4. Vertical field profiles of E_X along the z axis when the SPR structures possess dielectric gratings of $d_g = 0$, 100, and 200 nm.

Table 1. Enhancement Factors of SEF, SAGF, and OIEF When a Grating Period is 100 nm and its Thicknesses are 100 and 200 nm

Enhancement	$d_g = 100$ nm	$d_g = 200$ nm
SEF	2.6	3.0
SAGF	3.0	5.0
OIEF	2.4	2.9

B. Effect of Grating Period on Sensitivity Enhancement

Reduction of a grating period Λ is another effective way to increase the surface reaction area. While it is required to develop a high-resolution manufacturing process for fabricating subwavelength nanostructures, the recent advance in plasmonics allows us to open up the possibilities of nanostructuring the substrates in a controllable way [16]. For example, nonconventional lithographic techniques such as nanoimprint lithography (NIL) and nanosphere lithography can be used to generate largely patterned areas of sub-100 nm resolution at a low cost. Since NIL is based on the direct mechanical deformation of the resist, the resolution achievable with NIL is beyond the limitations caused by light diffraction or beam scattering in other optical lithographies. It has been experimentally demonstrated that nanoscale patterns as small as 10 nm could be successfully transferred by this method [17].

Considering the achievable feature size in NIL-based fabrication, we investigate the effect of the grating period on the sensitivity enhancement in a wide range of 50 nm $\leq \Lambda \leq$ 1000 nm. It is clearly observed in Fig. 5 that when d_g is fixed at 50 nm, the correlation between SEF and SAGF is very strong over the whole range of the grating period. In particular, the SEF displays an exponential growth from 1.05 for $\Lambda = 1000$ nm to 1.21 for $\Lambda = 400$ nm, 1.53 for $\Lambda = 200$ nm, 2.00 for $\Lambda = 100$ nm, and 3.11 for $\Lambda = 50$ nm. As Λ decreases, overall surface area tends to be larger and this can induce a notable amplification of the SPR signal.

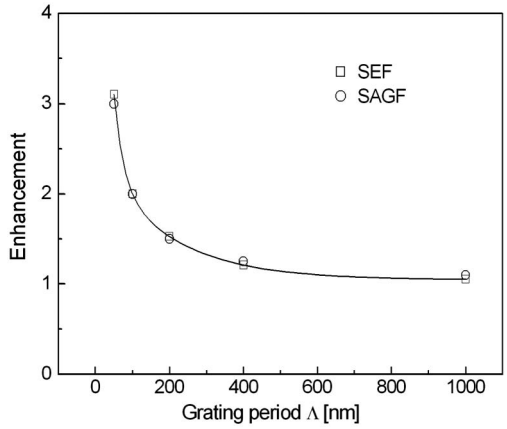

Fig. 5. Correlation analysis between SEF (rectangle) and SAGF (circle) for a thin grating of $d_g = 50$ nm when Λ changes from 50 to 1000 nm.

Figure 6 presents the SEF characteristics for $\Lambda = 50$, 100, 200, and 400 nm, as a function of the grating thickness, and a few notes are worth a look in the results. First of all, the qualitative trends of increased SEF with a larger grating thickness resemble the results discussed in Subsection 3.A. It is attributed to the fact that thicker gratings can provide more rooms for target analytes attached to the sensor substrate. Moreover, when a grating thickness is larger than 100 nm, the rate of SEF growth becomes lower and finally decreases to zero. Limited penetration depth of plasmon waves tends to suppress further increase of sensitivity characteristics, so that the structure stops improving the sensitivity performance of the SPR biosensor.

Special attention should be given to an abrupt reduction of SEF at the period of $\Lambda = 200$ nm. It is possibly due to an effect of radiation damping, which indicates that the incident light is interfered by the diffracted beam [18]. When the grating vector $K(= 2\pi/\Lambda)$ and the wavevector k_{SPR} satisfy $K = 2k_{\mathrm{SPR}}$, one backward diffraction order is generated by the grating, and it propagates with an angle of θ_{SPR}, which can be described by

$$K = \frac{2\pi}{\Lambda} = 2k_{\mathrm{SPR}} = 2k_0\sqrt{\varepsilon_p}\,\sin\,\theta_{\mathrm{SPR}}, \qquad (2)$$

where ε_p is a dielectric constant of glass prism. At this condition, the diffracted light has a reflection angle of θ_{SPR}, and its trace exactly overlaps the incidence beam. As a result, the incident beam can be highly degenerated through a destructive coupling between the incidence and the diffracted light. Since intensity of the diffracted beam is strong enough to be comparable to the incidence, SPR characteristics can be affected significantly. Figure 7(a) shows the dependence of a resonance angle on the grating thickness at $\Lambda = 200$ nm before and after target binding event. For both cases, the resonance angles are determined in the range of $60° < \theta_{\mathrm{SPR}} < 70°$. If these SPR characteristics are compared with the data in Fig. 7(b), the curve $K = 2k_{\mathrm{SPR}}$ at around

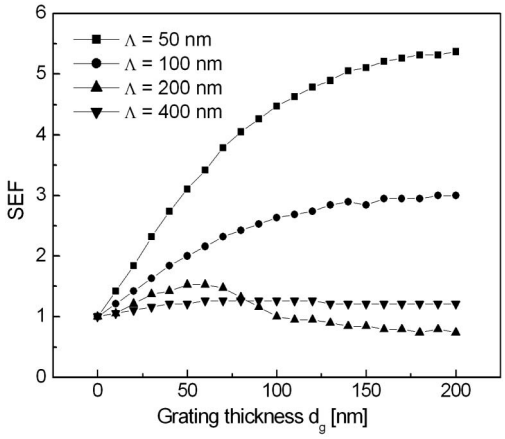

Fig. 6. SEF characteristics with respect to the grating period Λ when grating thickness d_g increases.

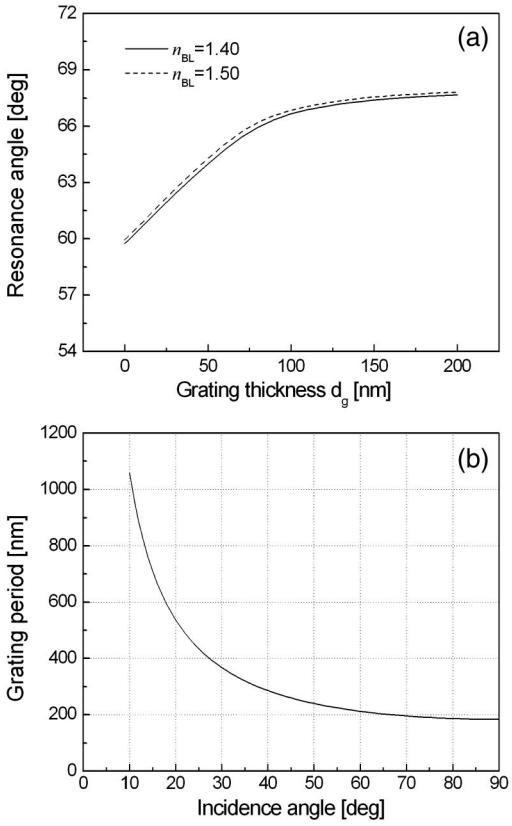

Fig. 7. (a) Resonance angles as a function of the grating thickness at $\Lambda = 200$ nm before and after target binding and (b) the condition satisfying $K = 2k_{\mathrm{SPR}}$. Along the curve of $K = 2k_{\mathrm{SPR}}$, the radiative damping effect is caused by the interference between the incidence and the diffracted light.

$\Lambda = 200$ nm corresponds well with the resonance angle range in which an abrupt change in SEF profile is observed in Fig. 6. It should be also emphasized that, when $\Lambda = 200$ nm and $d_g > 100$ nm, the SEF value becomes smaller than 1, implying that the use of subwavelength gratings may degrade the sensitivity performance, compared to a conventional SPR configuration. Hence, in actual SPR implementation, dielectric grating structures should be carefully designed to avoid such radiative damping.

C. Effect of Chromium Adhesion Layer on Sensitivity Enhancement

In terms of an actual production of dielectric subwavelength gratings on a metal film, one may take advantage of the molding technique based on NIL. Although implementing the geometric parameters of the grating molds with a high precision and achieving a uniform pattern in a reproducible manner remain a challenge, the relevant experimental work is currently under way in our group. For example, a gold film is evaporated onto an SF10 glass substrate after an evaporation of chromium adhesion layer. A silicon dioxide (SiO_2) layer is then grown on the gold film via the thermal oxidation method. After the nanoscale patterning process of transferring the imprinted patterns, a large-area stamp with

high feature density can create a deep thickness contrast in the imprint resist. Subsequently, the dielectric SiO_2 grating is formed by anisotropic dry etching with a 9:1 C_4F_8–O_2 mixture, and the lift-off approach can be utilized to remove the patterned residual polymers.

In the fabrication process of designed dielectric gratings, a thickness control of the adhesion layer is another important issue for successful realization of grating-based SPR samples. The thin transition metal films, such as chromium, titanium, and tungsten are generally employed as an adhesion promoter between the noble metal film and the glass substrate [19]. They not only improve the adhesion but also enhance the stability of the noble metal film. If the adhesion film is not used, the metal film supporting plasmon excitation can be peeled off or damaged by severe processes, such as oxidation and dry etching and/or subsequent SPR experiments. On the other hand, when a thick adhesion is employed, SPR characteristics can be degenerated by a large imaginary part of its complex dielectric constant. In this section, the influences of the thickness of chromium adhesion film on the sensor performance will be briefly explored.

When a thickness of gold film is 45 nm and a dielectric grating has a period of $\Lambda = 100$ nm and $f = 0.5$, the resonance angle shift before and after binding events is numerically calculated for a wide range of chromium thickness. According to Fig. 8(a), the sensitivity characteristic does not change significantly as the thickness of chromium layer increases up to 15 nm. On the one hand, the influence of chromium layer is prominent only at a thickness over 20 nm. On the other hand, the chromium layer affects the reflectance at a resonance angle more dominantly. In Fig. 8(b), in contrast to the case of adhesion thickness less than 5 nm showing an almost complete absorption in the SPR curve, the minimum reflectance increases notably with the adhesion layer when the thickness is greater than 5 nm, which is attributable to a high absorption property of chromium. Although the contribution of the chromium film is not constant as d_g increases, it is obviously observed that the influence of the chromium becomes stronger as an adhesion thickness increases. In particular, since increment in reflectance may aggravate the uncertainty of the sensor output and affect a high standard error in experiments, the maximally allowable thickness of the chromium layer should not exceed 5 nm.

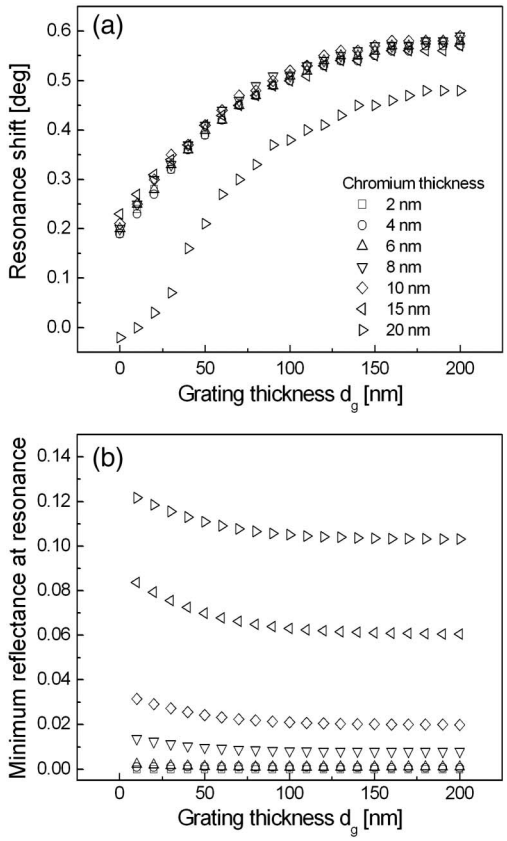

Fig. 8. Sensor performance of (a) resonance angle shift and (b) minimum reflectance as the thickness of chromium film increases. The dielectric gratings have a period of $\Lambda = 100$ nm and $f = 0.5$.

4. Discussion

This section demonstrates that the proposed SPR design with a dielectric grating may yield better sensing performance than the SPR scheme with a metallic grating. For comparison study, a grating period is fixed at $\Lambda = 50$ nm, based on the previous results that an extremely sensitive plasmonic sensor typically requires metallic gratings of sub-50 nm linewidth [3]. First, an effect of grating thickness on the SPR characteristics is investigated for metallic and dielectric gratings. As mentioned in Section 1, we find in Fig. 9(a) that reflectance curves for metallic gratings are significantly distorted depending on the grating thickness d_g, which is associated with a multiple excitation of localized plasmon modes occurring at the metallic gratings and their destructive interference with propagating SP modes [5]. As the grating thickness increases, a broader and shallower dip at resonance makes detection of binding events insensitive and inaccurate. Hence, the optimal metallic grating is determined at $d_g = 5$ nm and its sensitivity improvement of 5.7 times is obtained, compared with a thin-film-based SPR system without any gratings.

On the other hand, Fig. 9(b) shows that the curve width and the minimum reflectance in SPR curves for dielectric gratings are not significantly influenced by the growing d_g. In addition to such sharp and deep SPR curves, the SPR sensor system with a dielectric grating can provide a noteworthy sensitivity enhancement. From our RCWA calculations, enhanced sensitivity over 4.5 times is achieved by a dielectric grating of $d_g > 100$ nm, and the highest improvement up to 5.4 times is obtained at the maximum thickness of $d_g = 200$ nm. More importantly, as a dielectric grating-based SPR structure can offer an

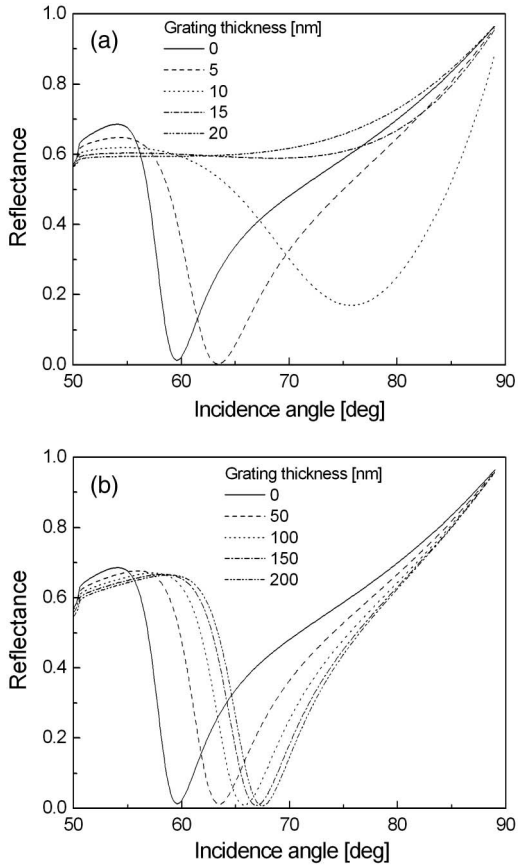

Fig. 9. Reflectance curves of SPR biosensors with (a) metallic and (b) dielectric gratings when $\Lambda = 50$ nm and $f = 0.5$. The solid curves indicate the results of a thin-film-based SPR system without grating structures.

improved sensitivity at a wide range of grating thickness, it enables better performance reliability and robustness to fabrication errors than the metallic grating-based one.

Subsequently, in order to evaluate an overall sensor performance more quantitatively, we employ a figure of merit (FOM) as follows:

$$\mathrm{FOM} = \frac{m[\mathrm{deg}/\mathrm{RIU}]}{\mathrm{FWHM}[\mathrm{deg}]} \cdot (1 - \mathrm{MRR}),$$

where m is the slope of the resonance angle over a refractive index range in the binding site, which corresponds to the sensor sensitivity. The FOM is a quality factor that takes the full width at half-maximum (FWHM) and the minimum reflectance at resonance (MRR) into account. A smaller FWHM and a lower MRR are, therefore, required because a deeper and narrower resonance peak allows an efficient detection of resonance shift and a precise analysis of sensing events.

Based on an assumption that the refractive index n_{BL} of a 2 nm thick binding layer with a uniform coverage varies from 1.40 to 1.50 in PBS solution, the SPR biosensor with a metallic grating of $\Lambda = 50$ nm and $d_g = 5$ nm is found to have a FOM value of 1.12, while a conventional SPR system without grating structures has a FOM = 0.25. Figure 10 shows FOM results for the proposed SPR structure when the thickness of a dielectric grating increases. The FOM value displays a gentle increment because the change in d_g causes the sensor sensitivity m to increase, while FWHM and MRR are not highly affected by the grating thickness. In particular, note that, when d_g is larger than 140 nm, the SPR biosensor with a dielectric grating exhibits greater sensing performance than the one with an optimized metallic grating.

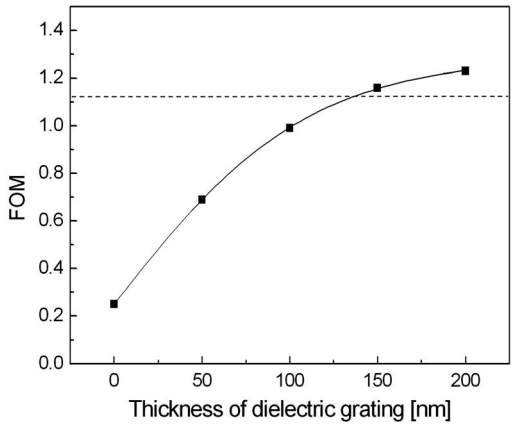

Fig. 10. FOM values of the dielectric-grating-based SPR system. The dotted line indicates the FOM value of the SPR sensor with a metallic grating of $\Lambda = 50$ nm and $d_g = 5$ nm.

5. Conclusion

In this study, we have investigated the sensitivity improvement of SPR detection by incorporating subwavelength dielectric gratings. Using the RCWA method, we have calculated the SEF dependence on the geometric parameters of the grating, such as thickness and period. Theoretical results showed that larger SEF can be feasible by increasing the thickness and reducing the period, which is associated with the increased surface reaction area. An abrupt fluctuation in SEF characteristic at $\Lambda = 200$ nm was clarified based on the radiative damping effect. In particular, for quantitative analysis on the sensitivity enhancement, we employed the OI, and the strong correlation between OIEF and SEF was numerically verified. Finally, influence of chromium film on the sensor performance was studied. While the sensitivity of the resonance shift is not significantly affected by adhesion layer, the proposed SPR structure may suffer from an increase of minimum reflectance depending on a chromium thickness. This study could be helpful in optimizing the plasmonic substrate with subwavelength dielectric gratings toward an improvement of sensor sensitivity.

This work was supported by the National Research Foundation of Korea (NRF) grant funded by the Korea government (MEST) (2011-0029485).

References

1. J. Homola, "Surface plasmon resonance sensors for detection of chemical and biological species," Chem. Rev. **108**, 462–493 (2008).
2. X. D. Hoa, A. G. Kirk, and M. Tabrizian, "Towards integrated and sensitive surface plasmon resonance biosensors: a review of recent progress," Biosens. Bioelectron. **23**, 151–160 (2007).
3. K. Kim, D. J. Kim, S. Moon, D. Kim, and K. M. Byun, "Localized surface plasmon resonance detection of layered biointeractions on metallic subwavelength nanogratings," Nanotechnology **20**, 315501 (2009).
4. S. A. Kim, K. M. Byun, K. Kim, S. M. Jang, K. Ma, Y. Oh, D. Kim, S. G. Kim, M. L. Shuler, and S. J. Kim, "Surface-enhanced localized surface plasmon resonance biosensing of avian influenza DNA hybridization using subwavelength metallic nanoarrays," Nanotechnology **21**, 355503 (2010).
5. N.-H. Kim, W. K. Jung, and K. M. Byun, "Correlation analysis between plasmon field distribution and sensitivity enhancement in reflection- and transmission-type localized surface plasmon resonance biosensors," Appl. Opt. **50**, 4982–4988 (2011).
6. K. Ma, D. J. Kim, K. Kim, S. Moon, and D. Kim, "Target-localized nanograting-based surface plasmon resonance detection toward label-free molecular biosensing," IEEE J. Sel. Top. Quantum Electron. **16**, 1004–1014 (2010).
7. W. P. Hu, S.-J. Chen, K.-T. Huang, J. H. Hsu, W. Y. Chen, G. L. Chang, and K.-A. Lai, "A novel ultrahigh-resolution surface plasmon resonance biosensor with an Au nanocluster-embedded dielectric film," Biosens. Bioelectron. **19**, 1465–1471 (2004).
8. S. Wang, D. F. P. Pile, C. Sun, and X. Zhang, "Nanopin plasmonic resonator array and its optical properties," Nano Lett. **7**, 1076–1080 (2007).
9. S. Oh, J. Moon, T. Kang, S. Hong, and J. Yi, "Enhancement of surface plasmon resonance signals using organic functionalized mesoporous silica on a gold film," Sens. Actuators B **114**, 1096–1099 (2006).
10. S. Elhadj, G. Singh, and R. F. Saraf, "Optical properties of an immobilized DNA monolayer from 255 to 700 nm," Langmuir **20**, 5539–5543 (2004).
11. E. D. Palik, *Handbook of Optical Constants of Solids* (Academic, 1985).
12. M. G. Moharam and T. K. Gaylord, "Rigorous coupled-wave analysis of metallic surface-relief gratings," J. Opt. Soc. Am. A **3**, 1780–1787 (1986).
13. L. Li and C. W. Haggans, "Convergence of the coupled-wave method for metallic lamellar diffraction gratings," J. Opt. Soc. Am. A **10**, 1184–1189 (1993).
14. N. Skivesen, R. Horvath, S. Thinggaard, N. B. Larsen, and H. C. Pedersen, "Deep-probe metal-clad waveguide biosensors," Biosens. Bioelectron. **22**, 1282–1288 (2007).
15. A. Shalabney and I. Abdulhalim, "Electromagnetic fields distribution in multilayer thin film structures and the origin of sensitivity enhancement in surface plasmon resonance sensors," Sens. Actuators A: Phys. **159**, 24–32 (2010).
16. W. K. Jung and K. M. Byun, "Fabrication of nanoscale plasmonic structures and their applications to photonic devices and biosensors," Biomed. Eng. Lett. **1**, 153–162 (2011).
17. A. Boltasseva, "Plasmonic components fabrication via nanoimprint," J. Opt. A: Pure Appl. Opt. **11**, 114001 (2009).
18. S. H. Choi, S. J. Kim, and K. M. Byun, "Design study for transmission improvement of resonant surface plasmons using dielectric diffraction gratings," Appl. Opt. **48**, 2924–2931 (2009).
19. S. Ekgasit, C. Thammacharoen, F. Yu, and W. Knoll, "Influence of the metal film thickness on the sensitivity of surface plasmon resonance biosensors," Appl. Spectrosc. **59**, 661–667 (2005).